Early Generation of New PrPSc on Blood Vessels after Brain Microinjection of Scrapie in Mice

Bruce Chesebro, James Striebel, Alejandra Rangel,* Katie Phillips, Andrew Hughson, Byron Caughey, Brent Race

Laboratory of Persistent Viral Diseases, Rocky Mountain Laboratories, NIAID, NIH, Hamilton, Montana, USA

* Present address: Alejandra Rangel, Pharmacology, University of Western Sydney, Campbelltown, NSW, Australia.

ABSTRACT Aggregation of misfolded host proteins in the central nervous system is believed to be important in the pathogenic process in several neurodegenerative diseases of humans, including prion diseases, Alzheimer's disease, and Parkinson's disease. In these diseases, protein misfolding and aggregation appear to expand through a process of seeded polymerization. Prion diseases occur in both humans and animals and are experimentally transmissible orally or by injection, thus providing a controllable model of other neurodegenerative protein misfolding diseases. In rodents and ruminants, prion disease has a slow course, lasting months to years. Although prion infectivity has been detected in brain tissue at 3 to 4 weeks postinfection (p.i.), the details of early prion replication in the brain are not well understood. Here we studied the localization and quantitation of PrPSc generation *in vivo* starting at 30 min postmicroinjection of scrapie into the brain. In C57BL mice at 3 days p.i., generation of new PrPSc was detected by immunohistochemistry and immunoblot assays, and at 7 days p.i., new generation was confirmed by real-time quaking-induced conversion assay. The main site of new PrPSc generation was near the outer basement membrane of small and medium blood vessels. The finding and localization of replication at this site so early after injection have not been reported previously. This predominantly perivascular location suggested that structural components of the blood vessel basement membrane or perivascular astrocytes might act as cofactors in the initial generation of PrPSc. The location of PrPSc replication at the basement membrane also implies a role for the brain interstitial fluid drainage in the early infection process.

IMPORTANCE Neurodegenerative diseases, including Alzheimer's disease, Parkinson's disease, and prion diseases, of humans are characterized by misfolding and aggregation of certain proteins, resulting in the destruction of brain tissue. In these diseases, the damage process spreads progressively within the central nervous system, but only prion diseases are known to be transmissible between individuals. Here we used microinjection of infectious prion protein (PrPSc) into the mouse brain to model early events of iatrogenic prion transmission via surgical instruments or tissue grafts. At 3 and 7 days postinjection, we detected the generation of new PrPSc, mostly on the outer walls of blood vessels near the injection site. This location and very early replication were surprising and unique. Perivascular prion replication suggested the transport of injected PrPSc via brain interstitial fluid to the basement membranes of blood vessels, where interactions with possible cofactors made by astrocytes or endothelia might facilitate the earliest cycles of prion infection.

Protein misfolding and aggregation in the central nervous system (CNS) appear to be key to the pathogenesis and progression of several neurodegenerative diseases of humans, including prion disease, Alzheimer's disease (AD), Parkinson's disease, frontotemporal dementia, and amyotrophic lateral sclerosis (1, 2). In all of these diseases, an aggregated misfolded host protein appears to accumulate progressively in certain CNS regions, resulting in a fatal outcome after a clinical phase usually lasting years. The specific host protein(s) involved in each of these diseases is different. However, the mechanisms of generation appear to be similar, as all involve seeded polymerization, where a misfolded aggregate binds and catalyzes misfolding of the normal isoform of the homologous protein (3). This allows the process to spread within the CNS. Although most neurodegenerative diseases are not transmissible between individuals, prion diseases are an exception, and spread of prion infection occurs naturally or experimentally in primates and other animals after exposure to infected tissue or fluids (4). The ability to initiate disease in experimental animals has made prion diseases a useful model for the study of aspects of other neurodegenerative diseases.

Prion diseases are slowly progressive in tempo, lasting months to years in rodents, ruminants, and primates. However, there is evidence of replication of the infectivity in the brains of mice and hamsters at 21 to 30 days after intracerebral injection (5–7). This early replication appears to precede the development of neuropathology. During prion disease, the CNS and lymphoid tissues ac-

cumulate an abnormal, disease-associated, typically protease-resistant form of prion protein, PrPSc, also known as PrPres or PrPd. PrPSc is derived from the normal host-encoded prion protein PrPC, also known as PrPsen (8). PrPSc is thought to play an important role in CNS damage, as it often colocalizes with vacuolation and gliosis in gray matter, which are the main pathological features of the disease (9–12).

Using various mouse prion disease models, previous studies have detected PrPSc in the brain as early as 35 to 70 days after intracerebral inoculation (13–17). Using mouse scrapie strain 22L, our group previously reported PrPSc and gliosis detectable by immunohistochemistry (IHC) assay at 40 days postinfection (p.i.) but not at 20 days p.i. (18). Early pathology and clinical signs have also been noted after stereotactic microinjection of scrapie strain ME7 into the hippocampus. In this model, early scrapie-induced neuroinflammation was seen at 56 days p.i., but PrPSc was not tested for (19). In another study by this same group, behavioral signs, as well as hippocampal PrPSc deposition and synaptic damage, were observed at 84 days p.i. (20), which was well in advance of the preterminal neurological clinical signs. In summary, in these mouse studies, PrPSc, astrogliosis, microgliosis, vacuolation, and clinical signs were not seen prior to 35 days p.i.

In the experiments described here, we studied very early events in the first minutes to days after infection in wild-type C57BL/10 (C57) mice. Little is known about how the brain initially reacts to the presence of infectious PrPSc introduced by intracerebral injection. Questions include whether there is an attempt by the host to eliminate the abnormally folded PrPSc in the inoculum and also how, when, and where the PrPSc inoculum begins to induce the formation of new PrPSc. Similar questions are also relevant to the initial spread of PrPSc generated by spontaneous conversion or by iatrogenic contamination from tissues or instruments or by the initial process of neuroinvasion from another site of primary infection. To address these issues, we microinjected 0.5 μl of a high concentration (10% brain homogenate [BH]) of 22L scrapie into C57 mice. This allowed us to detect the inoculum by IHC shortly after microinjection and also to follow the process of new PrPSc generation at very early time points. C57 mice were compared to PrP knockout (KO) control mice, which do not generate new PrPSc, and to C57 mice injected with normal BH (NBH). PrPSc was studied near the injection site in the striatum from 30 min to 40 days p.i. by IHC, immunoblot, and real-time quaking-induced conversion (RT-QuIC) assays for PrP amyloid seeding activity. Inoculated PrPSc appeared to be immediately transported to perivascular areas by the brain interstitial fluid (ISF) flow, and remarkably, new PrPSc was detectable as early as 3 to 7 days p.i.

RESULTS

Detection of 22L PrPSc by IHC assay at 30 min after microinjection into the striatum. To study the spread of prion infection in the brain on a microscopic scale, we microinjected 0.5 μl of 22L scrapie BH into the striata of wild-type C57 or PrP KO mice to initiate a small focal infection site (21). At 30 min p.i., PrPSc was detected by IHC staining with monoclonal antibody D13 in KO and C57 mice. In both mouse strains, PrPSc staining was not only located in the needle track (NT) wound but also observed in association with capillaries, veins, and arterioles in the striatum, corpus callosum, and cortex near the NT path (Fig. 1A and C). These perivascular sites and the white matter tracts are known sites of drainage of brain ISF (22). Thus, the injected PrPSc appeared to be rapidly collected by the ISF system for removal from the brain along with other solutes.

As controls, C57 and KO mice were also microinjected with 10% NBH, and these control mice showed no evidence of PrPSc staining in the NT regions (Fig. 1B and D). Thus, the staining observed in 22L-injected mice was specific for PrP from the 22L scrapie inoculum and was not found in the control NBH inoculum.

Detection of newly generated 22L PrPSc from as early as 3 days after microinjection into the striatum. Groups of 22L-injected mice were euthanized at various times postmicroinjection to follow the fate of the inoculated PrPSc and the generation of new PrPSc. At low magnification, PrPSc was seen near the NT at all of the time points tested from 30 min to 40 days p.i. (Fig. 2). Compared to the amount of D13 staining detected after 30 min (Fig. 2A), there was a marked reduction in staining in the NT after 3 days (Fig. 2B), suggesting that most of the PrP in the inoculum had been catabolized or removed, but small foci of perivascular D13 staining could be seen in the striatum. At 7 days p.i. and subsequent times up to 40 days p.i., the area and intensity of staining increased progressively around blood vessels of the striatum, cortex, and corpus callosum (Fig. 2C to F), suggesting that new PrPSc was being generated at those time points.

At 3 days p.i., at a higher magnification of the NT region, only minimal D13 staining was seen in 22L-injected KO mice (Fig. 3A), which indicated that most of the original inoculum was gone by that time. In contrast, in 22L-injected C57 mice, D13 staining was more abundant and was mostly perivascular (Fig. 3B, arrows). D13-positive blood vessels were detected at distances of up to 250 μm from the NT. This perivascular D13-stained material appeared to be newly generated PrPSc, as it differed considerably from the nonperivascular D13 staining seen in control NBH-injected C57 mice. In these control mice, a small amount of D13 staining in round structures, possibly axons, and in slightly larger irregular structures, possibly degenerating neurons, was seen near the NT (Fig. 3C). These structures were similar to PrP-stained structures detected by others at sites of hypoxic or toxic brain damage unrelated to prion disease, which are thought to be up-regulated PrPC in response to injury (23–25).

Microinjected mice were also analyzed at 7 days p.i. At that time, 22L-injected KO mice showed no detectable D13 staining (Fig. 3D). In contrast, in 22L-injected C57 mice, D13 staining was very prominent and was almost exclusively perivascular (Fig. 3E), although some staining was also noted around the edges of the healing NT. At 7 days p.i., in NBH-injected C57 mice, only rare D13 staining was noted (Fig. 3F) and its decrease by that time was in agreement with the interpretation that this PrP was a response to the needle stab injury. In summary, the presence of perivascular D13 staining in 22L-injected C57 mice and not in control NBH-injected mice strongly suggested that this material was newly generated PrPSc at both 3 and 7 days p.i.

Biochemical analysis of 22L-microinjected mice. To analyze the protease resistance of the PrP near the injection site, brain tissue in the region of the NT was dissected, homogenized, and analyzed for protease-resistant PrPSc by immunoblot assay with phosphotungstic acid (PTA) precipitation and a sensitive detection system (Femto). Low levels of proteinase K (PK)-resistant PrP were detected by immunoblot assay at 30 min and 1 day p.i. in some, but not all, 22L-injected C57 and KO mice (Fig. 4A and B). At 3 days p.i., the PrPSc signal was detectable in eight of nine
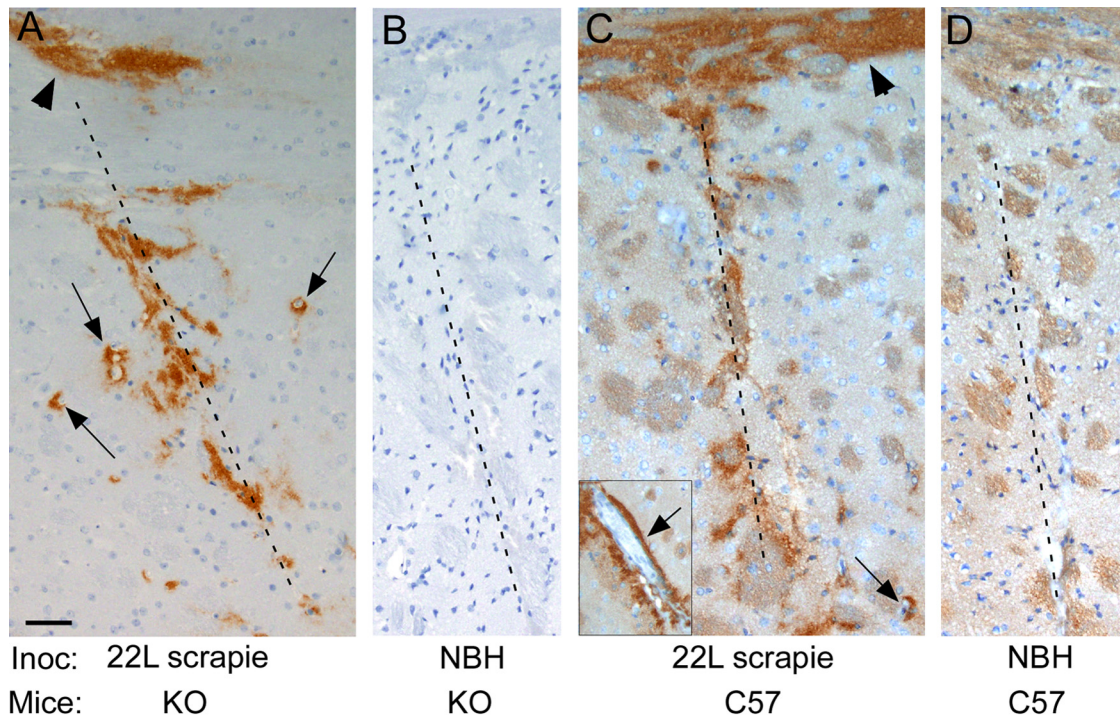
FIG 1 Detection of PrPSc in 22L scrapie inoculum (Inoc) at 30 min postmicroinjection by IHC assay with monoclonal antibody D13 directed against PrP. (A) In a KO mouse after the microinjection of 0.5 μl of 10% 22L scrapie BH, D13 staining was found in the NT wound in the striatum and also outside blood vessels (arrows) located up to 100 to 150 μm from the NT (dotted line), as well as in the white matter of the corpus callosum (arrowhead) near its crossing point with the NT. (B) No D13 staining was seen in a KO mouse after the injection of NBH. The NT with disturbed tissue is marked by a dotted line. (C) In a C57 mouse after the injection of 22L scrapie, D13 staining was noted on blood vessels (arrow), in the corpus callosum (arrowhead), and in structures at and near the NT wound (dotted line), similar to what was seen in KO mice. The inset shows prominent staining on a vessel that was just outside the field of view shown. (D) In a C57 mouse injected with NBH, no D13 staining of the input inoculum was seen. The light brown background staining seen in C57 mice, but not in KO mice, is due the presence of PrPsen in C57 mice. The scale bar in panel A is 50 μm, and the scale is the same for all of the panels. These panels are representative of multiple replicate mice, as detailed in Table 1.

C57 mice versus only three of nine KO mice (Fig. 4C). At 7 days p.i., eight of nine C57 mice had a strong signal (Fig. 4A and C), whereas none of the nine KO mice was positive (Fig. 4B and C). NBH-injected C57 mice at 1 day p.i. ($n = 3$), 3 days p.i. ($n = 4$), and 7 days p.i. ($n = 2$) were all negative for PrPSc by immunoblot assay (data not shown). The statistically significant difference in the incidence of PrPSc detection in 22L-infected C57 versus KO mice by immunoblot assay at both 3 and 7 days p.i. strongly suggested that new PrPSc was present at 3 and 7 days p.i.

The RT-QuIC assay is a highly sensitive method for the detection of PrP amyloid seeding activity in prion-infected tissues and cultures (26–28). Therefore, RT-QuIC was used to test some of the same samples used in the above-described immunoblot assays. PrP amyloid seeding activity was quantitated by testing quadruplicate wells of serial half-log dilutions for each mouse. An example is shown in which serial half-log dilutions were used, starting at $10^{-2.5}$ for a single mouse at 7 days p.i. In Fig. 4D, as the sample is diluted, the rise in the thioflavin T (ThT) signal level begins at progressively later times and the signal plateaus at lower levels. In Fig. 4E, the signal in each of four replicate wells at the 60-h time point is shown. From these data, the endpoint dilution giving 50% positive wells, i.e., the 50% seeding dose (SD_{50}), was calculated by the Spearman-Karber method and is plotted for each individual mouse in Fig. 4F. At 7 days p.i., the SD_{50} titer of C57 mice was 16-fold higher than that of KO mice ($P = 0.003$) (Fig. 4F). At 3 days p.i., the seeding activity was slightly higher in C57 mice, but

the difference from that in KO mice was not significant. Control C57 mice injected with NBH were also tested at 1, 3, and 7 days p.i. and were negative at those time points (data not shown), indicating that the D13-stained aggregates seen by IHC at 3 days p.i. in NBH-injected mice had no PrP amyloid seeding activity.

DISCUSSION

In the experiments described here, we studied the deposition, new generation, and spread of PrPSc *in vivo* near the NT in the striatum, corpus callosum, and cortex of the C57 mouse brain at very early times, starting at 30 min after scrapie microinjection. In our previous microinjection experiments with a 0.5-μl inoculum of 1% BH with scrapie strain RML, we were unable to visualize the inoculum at 30 min p.i., and new PrPSc was not detected until 40 days p.i. (21, 29). In the present studies, we injected a higher concentration (10%) of BH and also used the 22L scrapie strain, which had a 10-fold higher infectivity titer. With this combination, the injected PrPSc was visible at 30 min p.i. in both C57 and KO mice. This PrPSc was not only detected in the NT wound but also was seen surrounding numerous nearby small blood vessels, as well as within the adjacent corpus callosum white matter. These locations are known to be areas of drainage of CNS solutes in the brain ISF and are similar to the areas where we and others previously detected an ISF tracer, fluorescein isothiocyanate-ovalbumin, after similar microinjections (22, 30, 31).

The transport of PrPSc from the injection site to adjacent
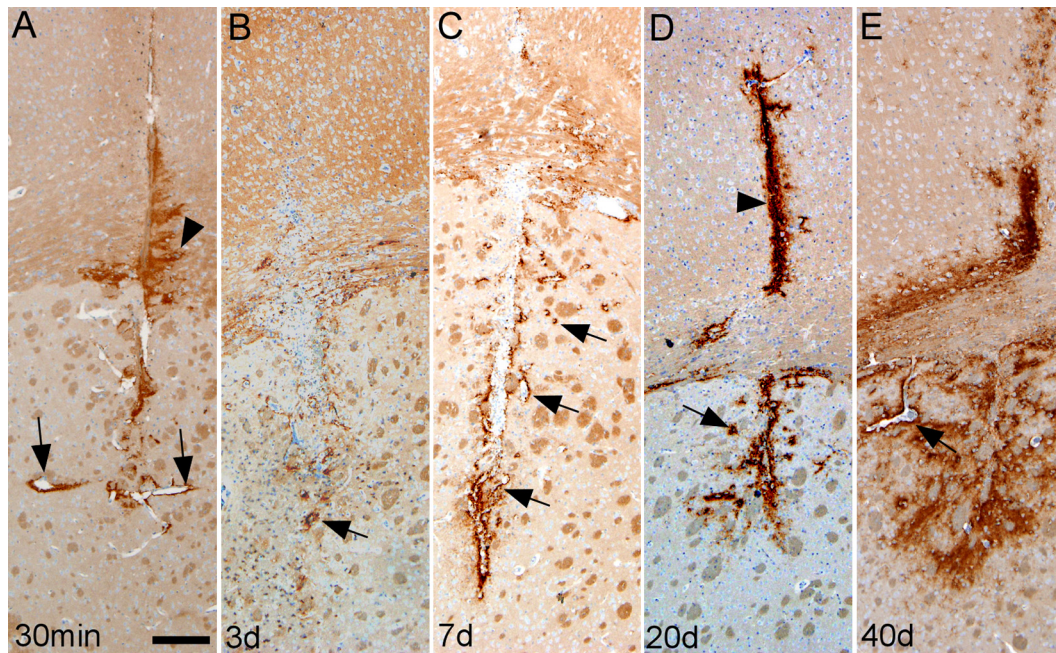
FIG 2 PrPSc detection in and near the NT from 30 min to 40 days postmicroinjection of C57 mice with 22L scrapie. (A) At 30 min p.i., D13 staining of the inoculum is seen in the striatum associated with blood vessels (arrows) and in the corpus callosum and cortex (arrowhead) near the NT. (B) At 3 days p.i., less D13 staining is seen near the NT, suggesting extensive clearance of the inoculum. However, some blood vessel-associated PrP (arrow) was visible in the striatum even at this low magnification. (C) At 7 days p.i., blood vessel- and wound-associated D13 staining (arrows) is more prominent than at 3 days p.i. (D) At 20 days p.i., stronger D13 staining was detected in the cortex, corpus callosum, and striatum. Numerous PrPSc-positive blood vessels were noted a short distance from the NT in the striatum (arrow). Dense D13 staining was seen in the NT in the cortex (arrowhead). (E) At 40 days p.i., extensive PrPSc was detected in a larger area of the cortex, corpus callosum, and striatum, often around vessels (arrow). The scale bar in panel A is 200 μm and applies to all of the panels. Similar findings were seen in multiple replicate mice (Table 1).

blood vessels by ISF flow within 30 min of injection was surprising, as we thought previously that most PrPSc particles might be larger than 500 kDa and thus too large to flow with the ISF (22). Possibly, most PrPSc aggregates were reduced to less than this size by sonication prior to injection or enzymatic cleavage *in vivo* after injection. Rapid disaggregation of PrPSc has been observed *in vitro* after uptake by cells (32). In our experiments with KO mice, there was additional evidence that PrPSc in the inoculum was catabolized or removed from the injection site, as it was no longer detectable by IHC or immunoblot assay by 7 days p.i. (Fig. 3D and 4B and C). However, with the more sensitive RT-QuIC test, low levels of PrP amyloid seeding activity from the inoculum were still detectable in KO mice at 7 days p.i.

Interestingly, in C57 mice at 3 and 7 days p.i., there was evidence by IHC assay of the generation of new PrPSc in perivascular locations near the injection site in the striatum. This was not seen in KO mice, which could not generate new PrPSc. Over the next 40 days p.i., the area of PrPSc IHC staining in C57 mice increased steadily mostly in perivascular locations in the striatum, as well as in the cortex and corpus callosum (Fig. 2). By immunoblotting, evidence of the early generation of new PrPSc was obtained at both 3 and 7 days p.i. (Fig. 4A to C). In addition, immunoblot assay data for both C57 and KO mice from 30 min and 1 day p.i. were weak and erratic, indicating that there was no selective trapping of the injected PrPSc by PrPC present in the C57 mice. Moreover, with the ultrasensitive RT-QuIC assay, which measures PrP amyloid seeding activity, a highly significant (16-fold) difference between C57 and KO mice was found at 7 days p.i. (Fig. 4F). Thus,

PrPSc generation does not appear to be a slow process *in vivo*. In support of this conclusion, experiments using lingual injection into hamsters (clinical endpoint, 77 days p.i.) detected PrPSc in the brainstem by IHC assay at 2 weeks p.i. (33). Our results were also consistent with increases in PrP amyloid seeding activity seen in brain tissue and cerebrospinal fluid from 10 to 30 days after the intracerebral injection of hamsters with 50-μl volumes of scrapie BH (34), as well as with early increases in PrP amyloid seeding activity in blood corresponding to new replication after the extranasal infection of hamsters (35).

The new PrPSc generation observed in this system was located mostly near the basement membrane (BM) region of capillaries, as well as small veins and arteries. This perivascular pattern of PrPSc deposition was similar to the cerebral amyloid angiopathy (CAA) seen in scrapie-infected tg44 transgenic mice, which express anchorless PrP (21). In this model, we previously proposed that smaller PrPSc aggregates capable of flowing with the ISF drainage toward the BM might interact with BM components such as glucosaminoglycans (36–38) or other cofactors (39–41) to increase the efficiency of new PrPSc generation, possibly via a scaffolding mechanism (29). Although the PrPSc in C57 mice is not amyloid, a similar scaffolding process might still occur in C57 mice. However, the ISF flow was not the only mechanism of prion spread in C57 mice, as we also noted typical long-distance PrPSc spread via neuronal circuitry to the ipsilateral thalamus and other areas by 40 days p.i. (data not shown).

In the experiments described here, in NBH-injected C57 mice at 3 and 7 days p.i., unusual dense PrP-staining material was de-
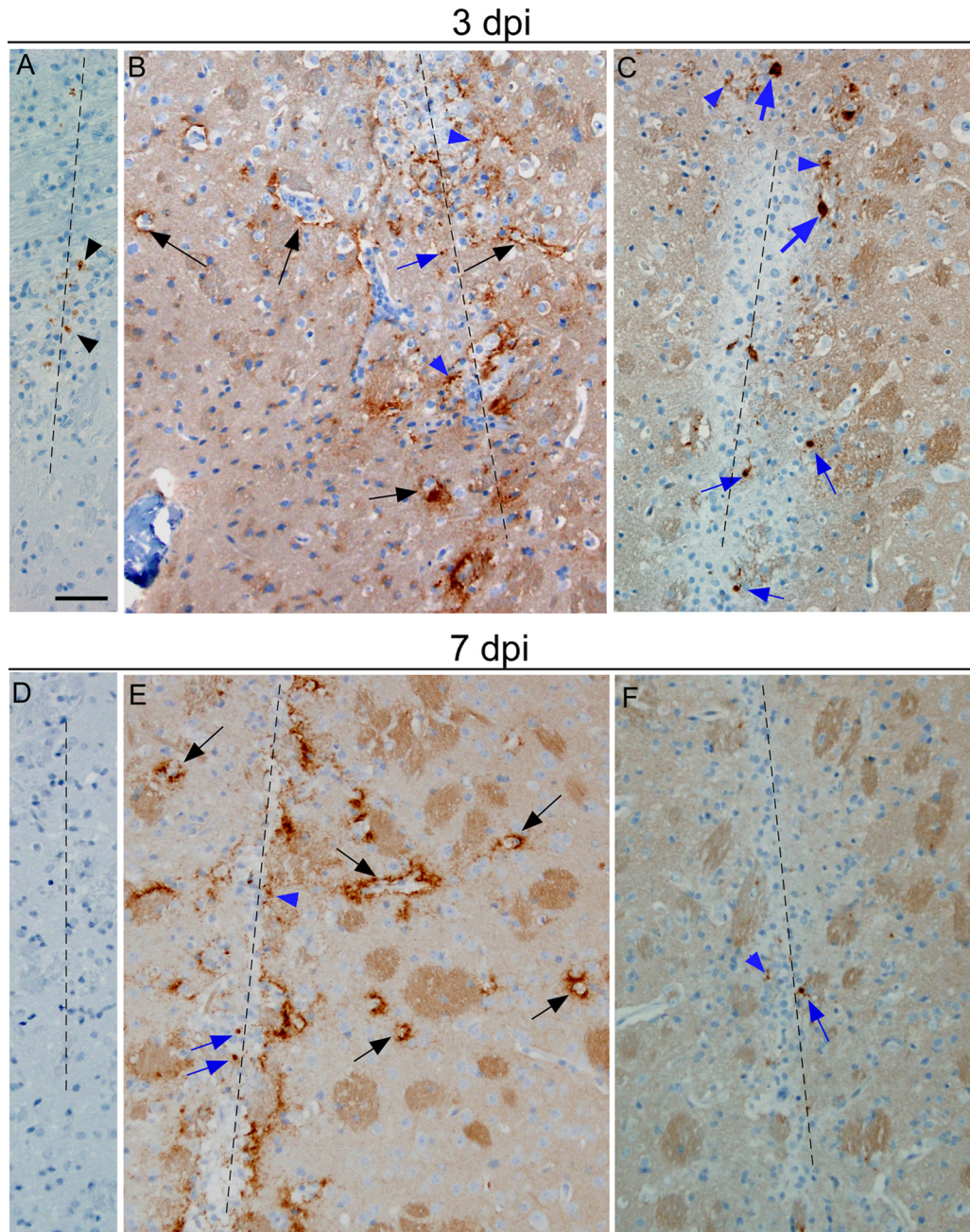
FIG 3 IHC analysis of PrP staining by D13 antibody at 3 (A to C) and 7 (D to F) days postmicroinjection of mice with 22L scrapie or NBH. The NT is indicated by the dotted line in each panel. (A) 22L-injected KO mouse showing a small amount of D13 staining (arrowheads) near the NT at 3 days p.i. (dpi). One other 22L-injected KO mice showed no detectable PrPSc at that time (not shown). (B) C57 mouse injected with 22L showing abundant D13 staining mostly around blood vessels (black arrows) in the NT area of the striatum at 3 days p.i. (arrows). On the basis of controls, most of this staining appeared to be new PrPSc generated at that time; however, a small amount of punctate staining (blue arrow) and diffuse staining (blue arrowheads) was similar to the staining in panel C and might be PrPC staining due to the needle stab wound (see below). (C) NBH-injected C57 mouse with D13 staining near the NT at 3 days p.i. D13 staining was observed in small round areas (blue arrows), slightly larger dense areas with projections (thick blue arrows), and some more diffuse areas (blue arrowheads). These structures resembled the PrPC staining previously reported to be degenerating axons and neurons in areas of hypoxic, metabolic, or inflammatory neurological damage, which was not related to prion disease (24, 25, 63). However, no perivascular D13 staining was seen in the NBH-injected control mice, and this difference distinguished these control mice from the 22L-injected C57 mice in panel B. (D) At 7 days p.i., in a 22L-injected KO mouse, no D13 staining was seen. (E) At 7 days p.i., a 22L-injected C57 mouse showed extensive perivascular D13 staining similar to that seen at 3 days p.i. (B). However, occasional punctate staining (blue arrows) and diffuse staining (blue arrowhead) were observed to be similar to panels C and F and were consistent with a PrPC response to the needle stab wound. (F) At 7 days p.i., an NBH-injected C57 mouse had a few areas of D13 staining of dense rounded structures (blue arrow) and some diffuse stained areas (blue arrowhead) similar to that seen in panel C, but no areas of perivascular D13 staining were detected. This result suggested that the injury-related PrPC response was almost at its end. In summary, at 7 days p.i., new PrPSc appeared to be more prominent than at 3 days p.i. Similar findings were seen in two to five replicate mice at each time point (Table 1), and each mouse was analyzed at two or three histological levels in the vicinity of the NT. The scale bar in panel A is 50 μm and applies to all of the panels.

tected near the edges of the NT (Fig. 3C and F). This staining was similar to some forms of bona fide PrPSc material but also appeared identical to the previously published PrPC staining associated with degenerating neurons and axons seen after hypoxic injury in mice and humans (24, 25, 42). Furthermore, the abnormal PrP in NBH-injected mice tested negative for both protease-resistant PrPSc and PrP amyloid seeding activity at 3 and 7 days p.i. (data not shown). Therefore, the abnormal PrP staining in NBH-injected mice was not PrPSc.

Intracerebral microinjection of brain extracts containing aggregated proteins associated with AD, Parkinson's disease, and frontotemporal dementia has also been shown to induce or accelerate the formation of misfolded protein aggregates by a prion-like seeded polymerization mechanism in several murine models. This seeding effect with A-beta (Aβ) or tau fibrils was effective only in transgenic mice expressing mutant APP or tau genes associated with increased AD or frontotemporal dementia in humans (43, 44), but α-synuclein (α-syn) fibrils were able to seed aggregation even in wild-type mice (45, 46). These processes were time dependent and were detectable as early as 2 weeks p.i. for tau and between 1 and 6 months p.i. for α-syn and Aβ. In the cases of α-syn and tau, the abnormal proteins were located inside neurons and were similar to aggregates seen in diseased humans (43, 47–49). In contrast, the amyloid Aβ aggregates often had a perivascular distribution similar to that of CAA noted in humans with AD (44, 50). However, recent evidence suggests that spread of Aβ amyloid might also occur via neuronal circuitry (51). Thus, the latter model was somewhat similar to our present results with scrapie-infected C57 mice, where perivascular PrPSc was the primary pattern observed from 3 to 40 days p.i. near the injection site but spread by neuronal circuitry to more distant sites was also evident at later times in disease (21).

The results in the present paper raise the question of why prion diseases are so slow (months to years), when PrPSc can begin replication rather rapidly after infection. Possibly, PrPSc needs to reach a certain minimum level before tissue damage occurs. There may also be particular CNS regions, such as the brainstem, where damage might have a more serious impact on clinical status. At later times, catabolism of PrPSc might be less effective because of aging or prior brain damage, leading to more rapid progression (52, 53). In addition, lower PrPC levels seen later in disease (54) might reduce the neuroprotective effects of PrPC that have been demonstrated in more acute damage models (24, 25). It is likely that a combination of these possibilities might influence the disease tempo, as none are mutually exclusive. However, the long time between the onset of PrPSc replication and detectable clinical damage leaves open a large window of opportunity for potential drug treatment. This approach would depend on having a noninvasive test for practical use on a large scale to facilitate early diagnosis and allow treatment to begin early, when its effectiveness would be greater. A similar strategy might also be effective in the other neurodegenerative diseases where prion-like protein aggregations occur.

MATERIALS AND METHODS

Ethics statement. All mice were housed at the Rocky Mountain Laboratory (RML) in an AAALAC-accredited facility in compliance with guidelines provided by the Guide for the Care and Use of Laboratory Animals (Institute for Laboratory Animal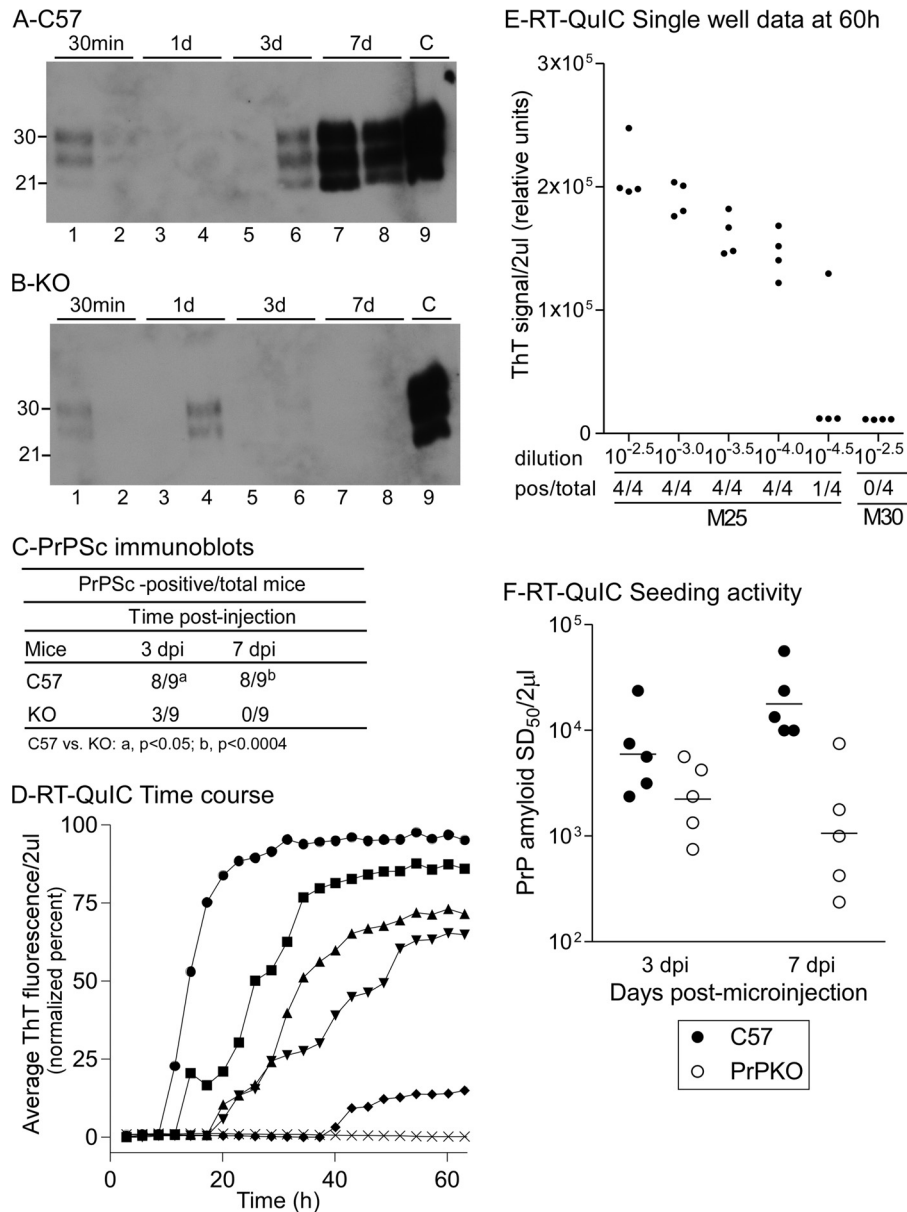 Research Council). Experimentation followed RML Animal Care and Use Committee-approved protocols 2011-04 and 2014-2023.

Experimental mice, scrapie strains, and tissue collection procedure. C57 mice were originally obtained from Jackson Laboratories and had been inbred at RML for several years. C57BL/10SnJ-Prnp$^{-/-}$ (PrP KO) mice were described previously in detail (55, 56). Young adult male mice weighing 26 to 30 g were used for all stereotactic inoculations. In order to inject a large amount of infectivity while producing a minimum of damage from the volume of inoculum used, mice were inoculated with 0.5 μl of a 10% 22L scrapie BH. The titer of this stock had been determined previously in C57 mice, and it contained 1.0×10^5 50% infective doses/0.5 μl. At selected time points postinoculation, mice were euthanized by isoflurane anesthesia overdose, followed by cervical dislocation. Their brains were removed and immersed in 10% neutral buffered formalin (3.7% formaldehyde) for histology. For future use in Western blot and RT-QuIC assays, the region surrounding the NT was dissected, isolated, and frozen in liquid nitrogen. Efforts were made to take the same amount of tissue (approximately 30 mg) from each NT region.

Stereotactic surgery and microinjection. Mice were anesthetized with isoflurane and positioned on a stereotaxic frame (David-Kopf Instruments, Tujunga, CA). A 1-cm midline incision was made in the skin over the dorsal surface of the skull, and the skull was exposed to allow the positioning of a drill over the bregma point of reference. From the bregma, the coordinates used were +1 mm anteroposterior, +1.7 mm lateral, and −3 mm ventral to the skull surface. These coordinates were selected to target the center of the left striatum and avoid passing through any ventricle. BHs were injected with Nanofil syringes (World Precision Instruments, Sarasota, FL) and steel bevel needles (33-gauge diameter; World Precision Instruments) into the striatum at a rate of 0.25 μl/min with a total of 0.5 μl per mouse controlled with a pump (UltraMicroPump III with a Micro4 pump controller; World Precision Instruments). The needle was kept in place for 2 min following injection to avoid any reflux of the BH solution. The skin incision was closed with sutures. These conditions produced minimal mechanical trauma to the brain. The patency of the needles was verified prior to and after injections. Mice were euthanized by isoflurane anesthesia overdose, followed by cervical dislocation, at different times after injection.

Immunoblot assay detection of PrPSc. Dissected brain tissue from the NT region (approximately 30 mg) was mixed with 270 μl of phosphate-buffered saline (PBS), and a 10% (wt/vol) BH was made with a Mini-Beadbeater homogenization system for 45 s on the homogenate setting. Following homogenization, 80 μl of each sample was removed and processed for RT-QuIC (see below). The remaining two-thirds of the BH from each NT sample (190 μl) was concentrated by a sodium PTA procedure adapted from a previously published method (57). BH was mixed with an equal volume of 4% Sarkosyl, vortexed, and incubated in a water bath at 37°C for 30 min. Benzonase (5 U/μl) and magnesium chloride (0.1 M) were then added to final concentrations of 50 U/ml and 0.001 M, respectively. Samples were vortexed and incubated in a water bath at 37°C for 45 min. Centrifugation at 5,000 × g for 5 min at room temperature was performed, and the supernatant was transferred to a new tube. PK was added to a final concentration of 50 μg/ml, and the mixture was vortexed and incubated in a water bath at 37°C for 1 h. The reaction was stopped with a 5 mM final concentration of Pefabloc. Four percent sodium PTA and 34 mM magnesium chloride, pH 7.4, were added to final concentrations of 0.3% and 2.56 mM, respectively, and the solution was incubated in a water bath at 37°C for 1 h. Samples were then centrifuged at 16,000 × g for 30 min at 37°C, and the supernatants were discarded. Pellets were then resuspended in 100 μl of PBS-EDTA (40 ml of 0.5 M EDTA and 60 ml of PBS, pH 7.4), incubated for 30 min in a 37°C water bath, and then centrifuged at 16,000 × g for 30 min at 37°C. The supernatants were again discarded, and the pellet was washed with 100 μl of PBS and incubated for 5 min in a 37°C water bath. A final centrifugation at 16,000 × g for 30 min at 37°C was performed, and the supernatant was discarded. The pellet was resuspended in 20 μl of Laemmli sample buffer,

A-C57

30 min | 1d | 3d | 7d | C

B-KO

30 min | 1d | 3d | 7d | C

C-PrPSc immunoblots

	PrPSc -positive/total mice	
	Time post-injection	
Mice	3 dpi	7 dpi
C57	8/9[a]	8/9[b]
KO	3/9	0/9

C57 vs. KO: a, p<0.05; b, p<0.0004

D-RT-QuIC Time course

E-RT-QuIC Single well data at 60h

F-RT-QuIC Seeding activity

FIG 4 Biochemical analysis of PrP in the NT region at 30 min and 1, 3, 7, and 40 days after the microinjection of NBH or scrapie strain 22L into C57 and KO mice. (A) Immunoblot assays of C57 mice at various times after 22L injection. Bands between 21 and 30 kDa are PrPSc. Lane 9 is a control NT sample from a C57 mouse at 40 days p.i. where only 1/8 of the usual sample amount was loaded. (B) Immunoblot assay of 22L-injected KO mice. Lane 9 is a control NT sample from a C57 mouse at 40 days p.i. where only 1/8 of the usual sample amount was loaded. Lanes C (control) in panels A and B at lower exposure times were used to verify similar quantitation on both gels. (C) Summary of PrPSc immunoblot assay results, including all of the mice tested at 3 and 7 days p.i. C57 mice differed significantly from KO mice at 3 days p.i. by Fischer's exact test. (D) RT-QuIC time course of PrP amyloid formation with dilutions of BH from a typical single C57 mouse microinjected with 22L at 7 days p.i. (M25). Dilutions: ●, $10^{-2.5}$; ■, $10^{-3.0}$; ▲, $10^{-3.5}$; ▼, $10^{-4.0}$; ◆, $10^{-4.5}$. Dilution for a control NBH-injected mouse (M30) at 1 day p.i., $10^{-2.5}$ (×). Similar negative data were seen in NBH-injected mice ($n = 3$) at dilutions of $10^{-2.5}$ to $10^{-4.5}$ as tested for 22L-infected mice (data not shown). Points represent the normalized average ThT fluorescence per 2 μl of each dilution from four replicate wells per dilution measured at multiple time points from 0 to 63 h. Note that the increase in ThT fluorescence occurred later with each progressive dilution. NBH-injected C57 mice were negative by RT-QuIC at 1 day p.i., which was the peak of the nonspecific injury response after injury by microinjection needle stab. (E) RT-QuIC data for single wells. Each point represents one replicate well at the 60-h time point for the dilutions indicated from mice 25 and 30. The number of positive wells/total number of wells tested at 60 h is shown below the dilution for each group of points. PrP amyloid seeding activity, expressed as the SD_{50} per 2 μl, was calculated from similar positive/total well data for all of the mice by the Spearman-Karber method as described in Materials and Methods, and the final data are shown in panel F for each mouse at 3 and 7 days p.i. (dpi). The difference between C57 and KO mice at 7 days p.i. was $10^{1.22}$, i.e., 16.6-fold, and was statistically significant ($P = 0.003$) by t test. At 3 days p.i., these groups were not statistically significantly different. Note that KO mice, which were negative by PrPres immunoblot assay, were positive by RT-QuIC assay. This is likely due to the sensitivity of the RT-QuIC method (59). In contrast, as shown in panel D, in NBH-injected mice at 1 day p.i. or in noninjected mice, no seeding activity was detectable at any time point up to 60 h for any of the dilutions tested ($10^{-2.5}$ to $10^{-4.5}$).

TABLE 1 Overview of the mice used per group in IHC studies of cellular accumulation of PrPSc at various time points after injection

Inoculum[a] and mouse strain[b]	No. of mice/group[c]					
	30 min	3 days	7 days	10 days	20 days	40 days
22L						
C57	5	2	5	3	5	6
KO	3	2	2	2		
NBH						
C57	3	2	2	3	3	3
KO	2			2		

[a] The inoculum was 0.5 μl of 10% scrapie BH or NBH.

[b] Mice were C57 or PrP KO on a C57 background, as described in Materials and Methods.

[c] The time points shown are minutes or days postinfection.

vortexed, and boiled for 5 min. The entire 20 μl (representing two-thirds of the original NT sample from each mouse) was loaded into a single lane on a 16% Tris-glycine gel and electrophoresed. Gels were transferred to polyvinylidene difluoride membranes with the iBlot transfer system (Life Technologies). Membranes were probed with a 1:100 dilution of human anti-PrP monoclonal antibody D13 derived from cell culture supernatants produced in our laboratory from CHO cells expressing the D13 antibody construct (21), which were kindly provided by R. Anthony Williamson. Monoclonal antibody D13 recognizes residues 94 to 105 of PrP (58) derived from mice, hamsters, and squirrel monkeys and has been extensively used for the detection of PrP in immunoblot and IHC assays. The secondary antibody was peroxidase-conjugated anti-human IgG at 1:10,000 (Sigma), and immunoreactive bands were visualized with a SuperSignal West Femto (Thermo Scientific) detection system.

Detection of PrP amyloid seeding activity by RT-QuIC assay. To detect PrP amyloid seeding activity by RT-QuIC assay, 10% BHs (80 μl as described above) were centrifuged at 2,000 $\times$ g for 2 min to remove large particulates. The remaining supernatants were aliquoted and frozen at $-80°C$ for RT-QuIC analysis at a later time. After thawing, supernatants were serially diluted in half-log ($10^{-0.5}$) increments from $10^{-2.5}$ to $10^{-4.5}$ with PBS, 0.05% SDS, and N2 medium supplement (1$\times$; Gibco), with the 10% BH designated the $10^{-1.0}$ dilution. Reactions were performed as previously described (28, 59) under the following assay conditions: 0.1 mg/ml mouse recombinant PrP substrate, 130 mM NaCl, 10 μM ThT, and 1 mM EDTA at 42°C (60). Four wells were subjected to RT-QuIC for each dilution. Each 100-μl reaction mixture was seeded with 2 μl of diluted sample, resulting in a final SDS concentration of 0.001% during incubation. The number of positive wells/total number of wells at each dilution for each sample was determined on the basis of ThT fluorescence at 60 h, and this value was used to calculate the seeding activity, which was defined as the inverse of the dilution giving positive reactions in 50% of the replicate wells, i.e., the SD_{50} per 2 μl of sample for each BH by using the Spearman-Karber formula for titer calculation (61).

Immunohistochemical detection of PrPSc. Brains were removed and placed in 10% neutral buffered formalin for 3 to 5 days. Whole brains were divided coronally into four regions, (i) the olfactory bulb to the bregma, including the entire striatum; (ii) the middle thalamic area; (iii) the midbrain, and (iv) the cerebellum. These tissues were then processed and embedded in paraffin. The block including the striatum was cut into 5-μm coronal sections through the entire striatum region. Every eighth section from the striatum was stained with hematoxylin and eosin to determine the NT location. Additional sections from the other three areas (thalamus, midbrain, and cerebellum) were obtained from mice at various time points as needed.

Sections were cut with a standard Leica microtome, placed on positively charged glass slides, and air dried overnight at room temperature. On the following day, the slides were heated in an oven at 60°C for 20 min. Deparaffinization, antigen retrieval, and staining were performed with the Ventana automated Discovery XT stainer. Because of the intense aggregation of PrPSc, immunostaining of PrPSc requires stringent antigen retrieval at high temperatures. In these experiments, PrPSc antigens were

exposed by incubation in CC1 buffer (Ventana) containing Tris-borate-EDTA, pH 8.0, for 100 min at 95°C as previously described (62). Staining for PrP was done with the human anti-PrP monoclonal antibody D13 described above. For the IHC assay, D13 culture fluid was used at a dilution of 1:100 for 2 h at 37°C. The secondary antibody was biotinylated goat anti-human IgG at a 1:250 dilution (Jackson ImmunoResearch, West Grove, PA), and streptavidin-biotin peroxidase was used with 3,3′-diaminobenzidine (DAB) as the chromogen (DAB Map kit; Ventana Medical Systems, Tucson, AZ). Hematoxylin was used as a counterstain for all slides. In the region of the NT, sections at two or three levels separated by 50 to 70 μm were analyzed to demonstrate the reproducibility of the findings.

In previous experiments comparing D13 with humanized monoclonal antibody D18, which recognizes PrP residues 133 to 157 (58), we found very similar patterns of PrPSc deposition in mouse scrapie infection models. Furthermore, in preliminary experiments with scrapie-infected Syrian hamsters or mice expressing hamster PrP (not shown), IHC results with antibody D13 were identical to results seen with antibody 3F4, which recognizes residues 107 to 112 of hamster PrP just C terminal to the D13 epitope.

The overall experimental plan and number of mice examined by pathology per group are shown in Table 1. In most cases, three or more mice per time point were examined, but occasionally when multiple time points were examined, only two mice were available. The photomicrographs shown in the figures are representative of typical fields seen in replicate mice. Slides were examined, and photomicrographs were taken and observed with an Olympus BX51 microscope and MicroSuite five software.

REFERENCES

1. **Caughey B, Lansbury PT**. 2003. Protofibrils, pores, fibrils, and neurodegeneration: separating the responsible protein aggregates from the innocent bystanders. Annu Rev Neurosci **26:**267–298. http://dx.doi.org/10.1146/annurev.neuro.26.010302.081142.
2. **Walker LC, Jucker M**. 2015. Neurodegenerative diseases: expanding the prion concept. Annu Rev Neurosci **38:**87–103. http://dx.doi.org/10.1146/annurev-neuro-071714-033828.
3. **Harper JD, Lansbury PT, Jr**. 1997. Models of amyloid seeding in Alzheimer's disease and scrapie: mechanistic truths and physiological consequences of the time-dependent solubility of amyloid proteins. Annu Rev Biochem **66:**385–407. http://dx.doi.org/10.1146/annurev.biochem.66.1.385.
4. **Aguzzi A, Polymenidou M**. 2004. Mammalian prion biology: one century of evolving concepts. Cell **116:**313–327. http://dx.doi.org/10.1016/S0092-8674(03)01031-6.
5. **Kimberlin RH, Walker CA**. 1979. Pathogenesis of mouse scrapie: dynam-

ics of agent replication in spleen, spinal cord and brain after infection by different routes. J Comp Pathol **89**:551–562. http://dx.doi.org/10.1016/0021-9975(79)90046-X.

6. **Kimberlin RH, Walker CA.** 1986. Pathogenesis of scrapie (strain 263K) in hamsters infected intracerebrally, intraperitoneally or intraocularly. J Gen Virol **67**:255–263. http://dx.doi.org/10.1099/0022-1317-67-2-255.

7. **Mould DL, Dawson AM, Rennie JC.** 1970. Very early replication of scrapie in lymphocytic tissue. Nature **228**:779–780. http://dx.doi.org/10.1038/228779a0.

8. **Caughey B, Baron GS, Chesebro B, Jeffrey M.** 2009. Getting a grip on prions: oligomers, amyloids, and pathological membrane interactions. Annu Rev Biochem **78**:177–204. http://dx.doi.org/10.1146/annurev.biochem.78.082907.145410.

9. **Budka H, Aguzzi A, Brown P, Brucher JM, Bugiani O, Gullotta F, Haltia M, Hauw JJ, Ironside JW, Jellinger K, et al.** 1995. Neuropathological diagnostic criteria for Creutzfeldt-Jakob disease (CJD) and other human spongiform encephalopathies (prion diseases). Brain Pathol **5**:459–466. http://dx.doi.org/10.1111/j.1750-3639.1995.tb00625.x.

10. **González L, Martin S, Begara-McGorum I, Hunter N, Houston F, Simmons M, Jeffrey M.** 2002. Effects of agent strain and host genotype on PrP accumulation in the brain of sheep naturally and experimentally affected with scrapie. J Comp Pathol **126**:17–29. http://dx.doi.org/10.1053/jcpa.2001.0516.

11. **Jeffrey M, Goodsir CM, Bruce ME, McBride PA, Fraser JR.** 1997. In vivo toxicity of prion protein in murine scrapie: ultrastructural and immunogold studies. Neuropathol Appl Neurobiol **23**:93–101. http://dx.doi.org/10.1046/j.1365-2990.1997.8498084.x.

12. **Parchi P, Giese A, Capellari S, Brown P, Schulz-Schaeffer W, Windl O, Zerr I, Budka H, Kopp N, Piccardo P, Poser S, Rojiani A, Streichemberger N, Julien J, Vital C, Ghetti B, Gambetti P, Kretzschmar H.** 1999. Classification of sporadic Creutzfeldt-Jakob disease based on molecular and phenotypic analysis of 300 subjects. Ann Neurol **46**:224–233.

13. **Büeler H, Raeber A, Sailer A, Fischer M, Aguzzi A, Weissmann C.** 1994. High prion and PrPSc levels but delayed onset of disease in scrapie-inoculated mice heterozygous for a disrupted PrP gene. Mol Med **1**:19–30.

14. **Diedrich JF, Bendheim PE, Kim YS, Carp RI, Haase AT.** 1991. Scrapie-associated prion protein accumulates in astrocytes during scrapie infection. Proc Natl Acad Sci U S A **88**:375–379. http://dx.doi.org/10.1073/pnas.88.2.375.

15. **Farquhar CF, Dornan J, Moore RC, Somerville RA, Tunstall AM, Hope J.** 1996. Protease-resistant PrP deposition in brain and non-central nervous system tissues of a murine model of bovine spongiform encephalopathy. J Gen Virol **77**:1941–1946. http://dx.doi.org/10.1099/0022-1317-77-8-1941.

16. **Jeffrey M, Martin S, Barr J, Chong A, Fraser JR.** 2001. Onset of accumulation of PrPres in murine ME7 scrapie in relation to pathological and PrP immunohistochemical changes. J Comp Pathol **124**:20–28. http://dx.doi.org/10.1053/jcpa.2000.0423.

17. **Tatzelt J, Groth DF, Torchia M, Prusiner SB, DeArmond SJ.** 1999. Kinetics of prion protein accumulation in the CNS of mice with experimental scrapie. J Neuropathol Exp Neurol **58**:1244–1249. http://dx.doi.org/10.1097/00005072-199912000-00005.

18. **Tribouillard-Tanvier D, Race B, Striebel JF, Carroll JA, Phillips K, Chesebro B.** 2012. Early cytokine elevation, PrPres deposition, and gliosis in mouse scrapie: no effect on disease by deletion of cytokine genes IL-12p40 and IL-12p35. J Virol **86**:10377–10383. http://dx.doi.org/10.1128/JVI.01340-12.

19. **Betmouni S, Perry VH.** 1999. The acute inflammatory response in CNS following injection of prion brain homogenate or normal brain homogenate. Neuropathol Appl Neurobiol **25**:20–28. http://dx.doi.org/10.1046/j.1365-2990.1999.00153.x.

20. **Cunningham C, Deacon R, Wells H, Boche D, Waters S, Diniz CP, Scott H, Rawlins JN, Perry VH.** 2003. Synaptic changes characterize early behavioural signs in the ME7 model of murine prion disease. Eur J Neurosci **17**:2147–2155. http://dx.doi.org/10.1046/j.1460-9568.2003.02662.x.

21. **Rangel A, Race B, Phillips K, Striebel J, Kurtz N, Chesebro B.** 2014. Distinct patterns of spread of prion infection in brains of mice expressing anchorless or anchored forms of prion protein. Acta Neuropathol Commun **2**:8. http://dx.doi.org/10.1186/2051-5960-2-8.

22. **Rangel A, Race B, Striebel J, Chesebro B.** 2013. Non-amyloid and amyloid prion protein deposits in prion-infected mice differ in blockage of interstitial brain fluid. Neuropathol Appl Neurobiol **39**:217–230. http://dx.doi.org/10.1111/j.1365-2990.2012.01303.x.

23. **Jeffrey M, Scholes SF, Martin S, McGovern G, Siso S, Gonzalez L.** 2012. Increased immunohistochemical labelling for prion protein occurs in diverse neurological disorders of sheep: relevance for normal cellular PrP function. J Comp Pathol **147**:46–54. http://dx.doi.org/10.1016/j.jcpa.2011.08.011.

24. **McLennan NF, Brennan PM, McNeill A, Davies I, Fotheringham A, Rennison KA, Ritchie D, Brannan F, Head MW, Ironside JW, Williams A, Bell JE.** 2004. Prion protein accumulation and neuroprotection in hypoxic brain damage. Am J Pathol **165**:227–235. http://dx.doi.org/10.1016/S0002-9440(10)63291-9.

25. **Mitteregger G, Vosko M, Krebs B, Xiang W, Kohlmannsperger V, Nölting S, Hamann GF, Kretzschmar HA.** 2007. The role of the octarepeat region in neuroprotective function of the cellular prion protein. Brain Pathol **17**:174–183. http://dx.doi.org/10.1111/j.1750-3639.2007.00061.x.

26. **Atarashi R, Satoh K, Sano K, Fuse T, Yamaguchi N, Ishibashi D, Matsubara T, Nakagaki T, Yamanaka H, Shirabe S, Yamada M, Mizusawa H, Kitamoto T, Klug G, McGlade A, Collins SJ, Nishida N.** 2011. Ultrasensitive human prion detection in cerebrospinal fluid by real-time quaking-induced conversion. Nat Med **17**:175–178. http://dx.doi.org/10.1038/nm.2294.

27. **Orrú CD, Wilham JM, Raymond LD, Kuhn F, Schroeder B, Raeber AJ, Caughey B.** 2011. Prion disease blood test using immunoprecipitation and improved quaking-induced conversion. mBio **2**(3):e00078–11. http://dx.doi.org/10.1128/mBio.00078-11.

28. **Wilham JM, Orrú CD, Bessen RA, Atarashi R, Sano K, Race B, Meade-White KD, Taubner LM, Timmes A, Caughey B.** 2010. Rapid end-point quantitation of prion seeding activity with sensitivity comparable to bioassays. PLoS Pathog **6**:e1001217. http://dx.doi.org/10.1371/journal.ppat.1001217.

29. **Rangel A, Race B, Klingeborn M, Striebel J, Chesebro B.** 2013. Unusual cerebral vascular prion protein amyloid distribution in scrapie-infected transgenic mice expressing anchorless prion protein. Acta Neuropathol Commun **1**:25–36. http://dx.doi.org/10.1186/2051-5960-1-25.

30. **Carare RO, Bernardes-Silva M, Newman TA, Page AM, Nicoll JA, Perry VH, Weller RO.** 2008. Solutes, but not cells, drain from the brain parenchyma along basement membranes of capillaries and arteries: significance for cerebral amyloid angiopathy and neuroimmunology. Neuropathol Appl Neurobiol **34**:131–144. http://dx.doi.org/10.1111/j.1365-2990.2007.00926.x.

31. **Hawkes CA, Härtig W, Kacza J, Schliebs R, Weller RO, Nicoll JA, Carare RO.** 2011. Perivascular drainage of solutes is impaired in the ageing mouse brain and in the presence of cerebral amyloid angiopathy. Acta Neuropathol **121**:431–443. http://dx.doi.org/10.1007/s00401-011-0801-7.

32. **Choi YP, Priola SA.** 2013. A specific population of abnormal prion protein aggregates is preferentially taken up by cells and disaggregated in a strain-dependent manner. J Virol **87**:11552–11561. http://dx.doi.org/10.1128/JVI.01484-13.

33. **Bartz JC, Kincaid AE, Bessen RA.** 2003. Rapid prion neuroinvasion following tongue infection. J Virol **77**:583–591. http://dx.doi.org/10.1128/JVI.77.1.583-591.2003.

34. **Orrù CD, Hughson AG, Race B, Raymond GJ, Caughey B.** 2012. Time course of prion seeding activity in cerebrospinal fluid of scrapie-infected hamsters after intratongue and intracerebral inoculations. J Clin Microbiol **50**:1464–1466. http://dx.doi.org/10.1128/JCM.06099-11.

35. **Elder AM, Henderson DM, Nalls AV, Hoover EA, Kincaid AE, Bartz JC, Mathiason CK.** 2015. Immediate and ongoing detection of prions in the blood of hamsters and deer following oral, nasal, or blood inoculations. J Virol **89**:7421–7424. http://dx.doi.org/10.1128/JVI.00760-15.

36. **Caughey B, Brown K, Raymond GJ, Katzenstein GE, Thresher W.** 1994. Binding of the protease-sensitive form of PrP (prion protein) to sulfated glycosaminoglycan and Congo red [corrected]. J Virol **68**:2135–2141.

37. **Misumi Y, Ando Y, Ueda M, Obayashi K, Jono H, Su Y, Yamashita T, Uchino M.** 2009. Chain reaction of amyloid fibril formation with induction of basement membrane in familial amyloidotic polyneuropathy. J Pathol **219**:481–490. http://dx.doi.org/10.1002/path.2618.

38. **Wong C, Xiong LW, Horiuchi M, Raymond L, Wehrly K, Chesebro B, Caughey B.** 2001. Sulfated glycans and elevated temperature stimulate PrP(Sc)-dependent cell-free formation of protease-resistant prion protein. EMBO J **20**:377–386. http://dx.doi.org/10.1093/emboj/20.3.377.

39. **Deleault NR, Kascsak R, Geoghegan JC, Supattapone S.** 2010. Species-dependent differences in cofactor utilization for formation of the

protease-resistant prion protein in vitro. Biochemistry **49**:3928–3934. http://dx.doi.org/10.1021/bi100370b.

40. **Deleault NR, Piro JR, Walsh DJ, Wang F, Ma J, Geoghegan JC, Supattapone S**. 2012. Isolation of phosphatidylethanolamine as a solitary cofactor for prion formation in the absence of nucleic acids. Proc Natl Acad Sci U S A **109**:8546–8551. http://dx.doi.org/10.1073/pnas.1204498109.

41. **Supattapone S**. 2014. Elucidating the role of cofactors in mammalian prion propagation. Prion **8**:100–105. http://dx.doi.org/10.4161/pri.27501.

42. **Weise J, Crome O, Sandau R, Schulz-Schaeffer W, Bähr M, Zerr I**. 2004. Upregulation of cellular prion protein (PrPc) after focal cerebral ischemia and influence of lesion severity. Neurosci Lett **372**:146–150. http://dx.doi.org/10.1016/j.neulet.2004.09.030.

43. **Iba M, Guo JL, McBride JD, Zhang B, Trojanowski JQ, Lee VM**. 2013. Synthetic tau fibrils mediate transmission of neurofibrillary tangles in a transgenic mouse model of Alzheimer's-like tauopathy. J Neurosci **33**:1024–1037. http://dx.doi.org/10.1523/JNEUROSCI.2642-12.2013.

44. **Kane MD, Lipinski WJ, Callahan MJ, Bian F, Durham RA, Schwarz RD, Roher AE, Walker LC**. 2000. Evidence for seeding of beta-amyloid by intracerebral infusion of Alzheimer brain extracts in beta-amyloid precursor protein-transgenic mice. J Neurosci **20**:3606–3611.

45. **Luk KC, Kehm V, Carroll J, Zhang B, O'Brien P, Trojanowski JQ, Lee VM**. 2012. Pathological alpha-synuclein transmission initiates Parkinson-like neurodegeneration in nontransgenic mice. Science **338**:949–953. http://dx.doi.org/10.1126/science.1227157.

46. **Masuda-Suzukake M, Nonaka T, Hosokawa M, Oikawa T, Arai T, Akiyama H, Mann DM, Hasegawa M**. 2013. Prion-like spreading of pathological alpha-synuclein in brain. Brain **136**:1128–1138. http://dx.doi.org/10.1093/brain/awt037.

47. **Holmes BB, Furman JL, Mahan TE, Yamasaki TR, Mirbaha H, Eades WC, Belaygorod L, Cairns NJ, Holtzman DM, Diamond MI**. 2014. Proteopathic tau seeding predicts tauopathy in vivo. Proc Natl Acad Sci U S A **111**:E4376–E4385. http://dx.doi.org/10.1073/pnas.1411649111.

48. **Luk KC, Kehm VM, Zhang B, O'Brien P, Trojanowski JQ, Lee VM**. 2012. Intracerebral inoculation of pathological alpha-synuclein initiates a rapidly progressive neurodegenerative alpha-synucleinopathy in mice. J Exp Med **209**:975–986. http://dx.doi.org/10.1084/jem.20112457.

49. **Sanders DW, Kaufman SK, DeVos SL, Sharma AM, Mirbaha H, Li A, Barker SJ, Foley AC, Thorpe JR, Serpell LC, Miller TM, Grinberg LT, Seeley WW, Diamond MI**. 2014. Distinct tau prion strains propagate in cells and mice and define different tauopathies. Neuron **82**:1271–1288. http://dx.doi.org/10.1016/j.neuron.2014.04.047.

50. **Eisele YS, Obermüller U, Heilbronner G, Baumann F, Kaeser SA, Wolburg H, Walker LC, Staufenbiel M, Heikenwalder M, Jucker M**. 2010. Peripherally applied A{beta}-containing inoculates induce cerebral {beta}-amyloidosis. Science **330**:980–982. http://dx.doi.org/10.1126/science.1194516.

51. **Ye L, Hamaguchi T, Fritschi SK, Eisele YS, Obermüller U, Jucker M, Walker LC**. 9 February 2015. Progression of seed-induced Abeta deposition within the limbic connectome. Brain Pathol. http://dx.doi.org/10.1111/bpa.12252.

52. **Morimoto RI, Cuervo AM**. 2014. Proteostasis and the aging proteome in health and disease. J Gerontol A Biol Sci Med Sci **69**(Suppl 1):S33–S38. http://dx.doi.org/10.1093/gerona/glu049.

53. **Voisine C, Pedersen JS, Morimoto RI**. 2010. Chaperone networks: tipping the balance in protein folding diseases. Neurobiol Dis **40**:12–20. http://dx.doi.org/10.1016/j.nbd.2010.05.007.

54. **Mays CE, Kim C, Haldiman T, van der Merwe J, Lau A, Yang J, Grams J, Di Bari MA, Nonno R, Telling GC, Kong Q, Langeveld J, McKenzie D, Westaway D, Safar JG**. 2014. Prion disease tempo determined by host-dependent substrate reduction. J Clin Invest **124**:847–858. http://dx.doi.org/10.1172/JCI72241.

55. **Striebel JF, Race B, Chesebro B**. 2013. Prion protein and susceptibility to kainate-induced seizures: genetic pitfalls in the use of PrP knockout mice. Prion **7**:280–285. http://dx.doi.org/10.4161/pri.25738.

56. **Striebel JF, Race B, Pathmajeyan M, Rangel A, Chesebro B**. 2013. Lack of influence of prion protein gene expression on kainate-induced seizures in mice: studies using congenic, coisogenic and transgenic strains. Neuroscience **238**:11–18. http://dx.doi.org/10.1016/j.neuroscience.2013.02.004.

57. **Wadsworth JD, Joiner S, Hill AF, Campbell TA, Desbruslais M, Luthert PJ, Collinge J**. 2001. Tissue distribution of protease resistant prion protein in variant Creutzfeldt-Jakob disease using a highly sensitive immunoblotting assay. Lancet **358**:171–180. http://dx.doi.org/10.1016/S0140-6736(01)05403-4.

58. **Matsunaga Y, Peretz D, Williamson A, Burton D, Mehlhorn I, Groth D, Cohen FE, Prusiner SB, Baldwin MA**. 2001. Cryptic epitopes in N-terminally truncated prion protein are exposed in the full-length molecule: dependence of conformation on pH. Proteins **44**:110–118. http://dx.doi.org/10.1002/prot.1077.

59. **Vascellari S, Orrù CD, Hughson AG, King D, Barron R, Wilham JM, Baron GS, Race B, Pani A, Caughey B**. 2012. Prion seeding activities of mouse scrapie strains with divergent PrPSc protease sensitivities and amyloid plaque content using RT-QuIC and eQuIC. PLoS One **7**:e48969. http://dx.doi.org/10.1371/journal.pone.0048969.

60. **Groveman BR, Kraus A, Raymond LD, Dolan MA, Anson KJ, Dorward DW, Caughey B**. 2015. Charge neutralization of the central lysine cluster in prion protein (PrP) promotes PrP(Sc)-like folding of recombinant PrP amyloids. J Biol Chem **290**:1119–1128. http://dx.doi.org/10.1074/jbc.M114.619627.

61. **Dougherty RM**. 1964. Animal virus titration techniques, p 183–186. In Harris RJC (ed), Techniques in experimental virology. Academic Press, New York, NY.

62. **Klingeborn M, Race B, Meade-White KD, Rosenke R, Striebel JF, Chesebro B**. 2011. Crucial role for prion protein membrane anchoring in the neuroinvasion and neural spread of prion infection. J Virol **85**:1484–1494. http://dx.doi.org/10.1128/JVI.02167-10.

63. **Jeffrey M, Scholes SF, Martin S, McGovern G, Sisó S, González L**. 2012. Increased immunohistochemical labelling for prion protein occurs in diverse neurological disorders of sheep: relevance for normal cellular PrP function. J Comp Pathol **147**:46–54. http://dx.doi.org/10.1016/j.jcpa.2011.08.011.